1 # Migration and Differentiation of Osteoclast Precursors

2 # under Gradient Fluid Shear Stress

3 Y. Gao, T. Y. Li, Q. Sun, C. Y. Ye, M. M. Guo,

4 Z. B. Chen, J. Chen, B. Huo

5

6

7

8

9

10

11

12

13

14

15

16

17

18

19

20

21

22   **Abstract:** The skeleton is able to adapt to mechanical loading through bone

23   remodeling, i.e. bone resorption followed by bone formation. The osteoclasts close to

24   microdamages are believed to initiate bone resorption, but whether local mechanical

25   loading such as fluid flow regulates recruitment and differentiation of osteoclast

26   precursors at the site of bone resorption has yet to be investigated. In the present study,

27   finite element analysis first revealed that there exists low fluid shear stress (FSS) field

28   inside microdamage. Basing on a custom-made device of cone-and-plate fluid chamber,

29   finite element analysis and particle image velocimetry measurement were performed to

30   verify the formation of gradient FSS flow field. Furthermore, the effects of gradient

31   FSS on the migration, aggregation, and fusion of osteoclast precursors were observed.

32   Results showed that osteoclast precursor RAW264.7 cells migrate along radial

33   direction toward the region with lower FSS during exposure to gradient FSS

34   stimulation for 40 min, obviously deviating from the direction of actual fluid flow

35   indicated by fluorescent particles. When inhibiting calcium signaling pathway with

36   gadolinium and thapsigargin, cell migration toward low-FSS region was significantly

37   reduced. For other cell lines, MC3T3-E1, PDLF, rMSC and MDCK, gradient FSS

38   stimulation did not lead to the low-FSS-inclined migration. After being cultured under

39   gradient FSS stimulation for 6 days, the density of RAW264.7 cells and the ratio of

40   TRAP-positive multinucleated osteoclasts in low-FSS region were significantly

41   higher than those in high-FSS region. Therefore, osteoclast precursor cells may have

42   special ability to sense FSS gradient and tend to actively migrate toward low-FSS

43   region, which is regulated by calcium signaling pathway.

44   **Keywords:** gradient fluid shear stress; osteoclast precursor; migration; fusion;

45   calcium signaling pathway

Introduction

It has been well recognized that the skeleton is able to adapt to mechanical loading through bone remodeling, a process where mature bone tissue is removed followed by the formation of new bone tissue (1, 2). The removal of bone tissue at the early stage of bone remodeling is called bone resorption, which is mainly regulated by osteoclasts. Osteoclasts are multinucleated cells with the ability of dissolving bone mineral matrix. Mononuclear osteoclast precursors originate from hematopoietic stem cells and fuse into multinucleated mature osteoclasts under the activation of macrophage colony-stimulating factor (M-CSF) and Receptor Activator for Nuclear Factor-κ B Ligand (RANKL) (3). However, the recruitment or differentiation of osteoclast precursors at the site of bone resorption is still an unsolved problem.

Frost and his colleagues defined a specific anatomic structure of bone remodeling, basic multicellular unit (BMU), in which osteoclasts aggregate in and excavate the leading zone of BMU and osteoblasts deposit layers of osteoid in the reversal zone (1). It has been found that the resorption region characterized as BMU usually colocalizes with the microdamage in bone that forms after long-term cyclic mechanical loading (4, 5), which is called targeted bone remodeling (6). Further studies revealed that this colocation depends on the scale of microdamage. There are three types of microdamages in bone, i.e. linear microdamages, microdamages in a cross-hatched pattern, and diffuse damages (7, 8). The scale of linear or cross-hatched microdamages is approximately 10-100 μm, similar to or larger than that of osteoclasts (9); The size of diffuse damage is sub-micron, which is considerably less than that of osteoclasts. Some studies demonstrated that bone resorption usually occurs near large-scale microdamages (10-100 μm) rather than diffuse damage (10-12), but it remains unclear how osteoclast precursors migrate toward large-scale

3

71   microdamages and further fuse into mature osteoclasts.

72   Previous studies have revealed that mechanical factors are included in targeted

73   bone remodeling. For example, after inducing microdamage in the tibiae of

74   6-month-old rats, the number of resorption pits in weight-bearing animals was

75   significantly higher than that in hindlimb-suspended group (13). This finding

76   indicates that without the involvement of mechanical stimulations, chemical factors,

77   such as the secretion from apoptotic osteocytes, are insufficient to cause bone

78   remodeling around the microdamage. The deformation of bone mineral matrix caused

79   by mechanical loading can drive fluid flow within cavities, which further induces

80   fluid shear stress (FSS) on bone surface and adherent bone cells (14-16). Our previous

81   studies have shown that osteoclast precursors migrate along flow direction and

82   migration speed is proportional to the magnitude of FSS, which is regulated by

83   calcium signaling pathway (9, 17, 18). The FSS level in a microdamage should be less

84   than that on bone surface according to fluid mechanics (Fig. 1A), it therefore is

85   hypothesized that osteoclast precursors may migrate toward the low-FSS region, such

86   as around large-scale microdamages. The present study established the gradient FSS

87   field by using a custom-made cone-and-plate flow chamber, through which the

88   migration, aggregation, and differentiation of osteoclast precursors were observed and

89   analyzed.

90

91   ## Materials and Methods

92   **Cone-and-Plate Flow Chamber**

93   We designed and fabricated a cone-and-plate flow chamber to establish a flow

94   field with gradient wall FSS (Fig. 2A). This device mainly consists of motor, cone, and

95   regular six-well culture plate. The distance between the cone's tip and the plate surface

4

96   was controlled by placing a silicon membrane with thickness of 0.4 mm on plate

97   surface before fixing the cone and motor. The motorized rotation of the cone drives the

98   medium in culture plate to flow over cells cultured on the plate. Wall FSS exerted on

99   cells would be controlled by specifying the cone's rotation speed.

100

101   **Numerical Simulation**

102   Finite element (FE) analysis method was used for numerical simulation on flow

103   field. An FE model was constructed considering the geometric and physical parameters

104   of trabecular bone and microdamage (Fig. 1B). The length, width, and height of flow

105   channel is 800, 500, and 100 μm, respectively, which is similar to the typical distance

106   between the trabeculae (19). Furthermore, the grooves on the channel sidewall were set

107   to mimic microdamages on the trabeculae. The depth and width of a large groove were

108   100 μm and 50 μm, respectively, and those of the small groove were 10 μm and 20 μm,

109   respectively. The inlet and outlet pressures for this channel were assigned as 300 Pa

110   and 0 Pa, respectively, on the basis of pressure difference in the lacunar-canalicular

111   system (20). The mesh close to the grooves was locally refined to accurately simulate

112   the wall FSS therein (Figs. 1C and 1D).

113   For the model of cone-and-plate flow chamber (Fig. 2B), the cone's generatrix

114   was machined as polyline to establish a wall FSS field with constant gradient on the

115   plate surface. The radius of the polyline point R_s was 8 mm, and its vertical distance h_s

116   to the cone's tip was 0.05 mm. The total radius R_c of the cone was 16 mm, and its

117   vertical distance h_c to the tip was 0.15 mm. The gap h_0 between the cone's tip and the

118   plate surface was 0.4 mm. The angular velocity of the cone was 172 rpm. The radius

119   R of a well for the six-well culture plate was 17 mm. No-slip boundary condition was

120   assumed for all rigid surfaces in the model except for the cone, and a free-surface

121   boundary condition was used for the upper fluid surface within the well.

122   COMSOL Multiphysics software was adopted for FE analysis. Incompressible

123   viscous fluid in the above two models was assumed with density of 1×10^3 kg/m^{3}and

124   viscosity of 1×10^{-3} Pa·s. Digital image analysis was performed with ImageJ and

125   MATLAB software.

126

127   **PIV Experiment**

128   PIV technique was adopted to indicate the direction of fluid flow in the

129   cone-and-plate   flow   chamber   (Fig.2).   Briefly,   fluorescent   beads   of

130   carboxylate-modified polystyrene with mean diameter of 0.5 μm (Sigma, USA) were

131   suspended in deionized water (1:5) with a vortex mixer to ensure uniform distribution.

132   After the cone-and-plate flow chamber ran stably for 5 min under fluorescence

133   microscope, the movement of beads were recorded at 10 fps with a high-speed camera

134   at the focal plane 0.2 mm above the plate, which were shown as arc-like trajectory in

135   the images (Fig. 2D) (*Supplementary Movie S1*). The movement parameters of the

136   beads, including speed and orientation, were then analyzed by an image-processing

137   program based on MATLAB software.

138   PIV was also used to compute wall FSS close to the plate surface in the present

139   study. The trajectory of beads' movement was recorded at a focal plane 0.1 mm above

140   the plate surface (Fig. 2C). The linear velocity v_p was obtained by dividing the length

141   L_s of a trajectory arc with the exposure time of 0.1 s for one fluorescent image. Then

142   wall FSS $\tau_w = \eta \cdot v_p / h_p$, in which the distance h_p is 0.1 mm and the viscosity is

143   1×10^{-3} Pa·s. This wall FSS value was compared with that from numerical simulation.

144

6

Cell Culture

145

146   Osteoclast precursor RAW264.7 cells (European Collection of Cell Cultures, UK)

147   were cultured in Dulbecco's modified Eagle's medium (DMEM, Hyclone, USA)

148   supplemented with 10% fetal bovine serum (FBS, Gibco, USA), 100 unit/mL of

149   penicillin (Sigma, USA), and 100 unit/mL of streptomycin (Sigma, USA) at 37 °C and

150   5% CO_2. Osteoblast-like MC3T3-E1 cells and rat mesenchymal stem cells (rMSC)

151   (American Type Culture Collection, USA) were cultured in alpha-modified Eagle's

152   medium (Hyclone, USA) supplemented with 10% FBS, 100 unit/mL of penicillin, and

153   100 unit/mL of streptomycin. The culture method for periodontal ligament fibroblasts

154   (PDLF) and canine kidney epithelial cells (MDCK) (Peking Union Medical College

155   Hospital, China) was the same as RAW264.7 cells. Mononuclear RAW264.7 cells

156   were induced to fuse or differentiate into tartrate acid phosphatase (TRAP)-positive

157   multinucleated osteoclasts by 100 ng/mL RANKL (Bio-Techne, USA) and 30 ng/mL

158   M-CSF (Peprotech, USA). TRAP is a specific marker enzyme in osteoclasts.

159

Time-Lapsed Imaging for Cell Migration

161   To observe cell migration under fluid flow, cytosolic calcium ions were stained

162   with Oregon Green (Sigma, USA). The stock solution was prepared by mixing 50 μg

163   Oregon Green with18 μL 10% Pluronic F-127 (Eugene, USA) in DMSO. Cells were

164   seeded at density of 1×10^4 cell/mL in one well of six-well plate and then incubated with

165   the working solution, 2 μL stock solution of Oregon Green mixed with 1 mL DMEM

166   medium, for 1 h at 37 °C with 5% CO_2. The cells were washed three times with PBS

167   and then immersed in 3 mL DMEM medium. After the plate was connected with a

7

168   cone-and-plate device, live cell imaging was recorded for 40 min by 10 min intervals.

169   Finally, migration trajectory of each cell was observed, and the migration parameters,

170   including distance, speed and orientation, were analyzed.

171

172   **Inhibition of Calcium Signaling Pathways**

173   To study the effect of calcium signaling pathways on the migration of

174   RAW264.7 cells under gradient FSS, four pharmacological agents were employed.

175   Similar to our previous studies (17, 18), the agents were incubated with cells before

176   being exposed to FSS. In brief, 10 μM Gadolinium chloride (Gd, Sigma, USA) was

177   supplied as the blocker of mechanosensitive cation channel (MSCC). The calcium

178   stored in endoplasmic reticulum (ER) was depleted by 1 μM thapsigargin (TG, J&K

179   Chemicals, China). 10 μM U-73122 (Darmstadt, Germany) was adopted to inhibit

180   phospholipase C (PLC). For the above blocking tests, 10 min incubation of chemical

181   reagents was applied. Calcium-free DMEM medium (Gibco, USA) was used to

182   remove the extracellular calcium.

183

184   **Distribution and Differentiation of Cells under Long-Term Culture**

185   RAW264.7 cells were subjected to FSS three times each day and once for an hour

186   up to 6 days by using the cone-and-plate flow chamber. The chambers were placed in

187   cell incubator and maintained at 37°C with 5% CO_2. During this long-term culture, the

188   cells at different distances to the center were counted each day. To observe the fusion of

189   RAW264.7 cells, the cells on the culture plate were initially fixed with 4%

190   paraformaldehyde (Wako Pure Chemical Industries, Japan) for 15 min and were stained

191   with nuclear dye Hoechst (Eugene, USA) (PBS: Hoechst=1000:1) for 15 min at 37 °C

8

192   after washing three times with PBS. TRAP Staining Kit was used to identify the

193   formation of purple TRAP-positive, multinucleated osteoclasts.

194

195   **Statistical Analysis**

196   Data were presented as mean ± SD. Statistical analysis was performed using a

197   one-way analysis of variance with Tukey's post hoc test for multiple comparisons to

198   determine the statistical differences between the mean values of different groups. Each

199   group in this study was repeated at least three times. A value of $p < 0.05$ was considered

200   statistically significant.

201

202   # Results

203   **Cone-and-Plate Flow Chamber Provides Flow Field Similar to Physiological**

204   **Condition Close to Microdamage in Bone**

205   An FE model, containing grooves with different sizes on the sidewall of a fluid

206   channel, was established to investigate fluid flow field around microdamages in bone

207   (Fig. 1B). Simulation results showed that the FSS level inside the large or small

208   grooves is approximately 0.2 Pa, which is considerably lower than that of 1.6–1.8 Pa

209   in the main flow path (Fig. 1D and 1F). It was further shown that the gradient of wall

210   FSS on the bottom surface of large or small grooves ranges from 0 to 0.4 Pa/mm, and

211   it is less than 0.1 Pa/mm in the most region inside the large groove (Fig. 1G).

212   Cone-and-plate flow chamber was designed in this study to establish a

213   physiological gradient FSS field on the bottom of the plate. Figure 2E shows the

214   images of fluorescent beads at different locations away from the center and it can be

215   found that the lengths of the particles' trace are positively related to the distance. The

216   calculated wall FSS displayed a linear relation with the distance, ranging from 0.1 Pa

9

217   to 0.7 Pa, and the fitted gradient is 0.6 Pa/mm (Fig. 3B). Numerical simulations also

218   revealed low-FSS level in the center of culture plate (Fig. 3A) with the fitted gradient

219   similar to PIV measurements (Fig. 3B). This FSS level and its gradient were selected to

220   mimic the physiological FSS values of less than 3 Pa for bone cells (21) and to consider

221   the above FE simulation result for large groove in Fig. 1G.

222   The velocity vectors of fluid flow at a specific point 10 μm away from the plate's

223   center are shown in Fig. 3C. It can be found that secondary flow deviating primary

224   flow along circumferential direction was produced in the cone-and-plate flow

225   chamber. PIV technique was adopted to experimentally indicate flow direction in the

226   chamber (Figs. 2C and 2D). The average angles of flow direction relative to

227   circumferential direction obtained from the FE analysis and PIV measurement were

228   8.3° and 7.0°, respectively, and no significant difference was observed between them

229   (Fig. 3D).

230

231   RAW264.7 Cells Migrate toward Low-FSS Region

232   After being stained with Oregon Green, the migration of RAW264.7 cells

233   responding to gradient FSS was recorded for 40 min (Fig. 4A), and the images were

234   captured at 6 mm away from the plate center (Fig. 4B; Supplementary Movies S2 and

235   S3). The wall FSS at this region was approximately 0.4 Pa. The definition of migration

236   parameters is shown in Fig. 4C. It can be found that the average angle of cell migration

237   relative to circumferential direction after 40-min-FSS stimulation was approximately

238   90°, which was significantly larger than 69° or 75° after 10-min or 20-min FSS

239   stimulation (Fig. 4D). No significant difference was observed for migration speed in all

240   time periods, which ranges from 0.18 μm/min to 0.23 μm/min (Fig. 4E). The angle of

241   cell migration relative to circumferential direction was considerably larger than that of

242   secondary flow in Fig. 3D, suggesting that the migration of cells toward low-FSS

243   region is not driven directly by fluid flow. When chemically blocking MSCC, PLC or

244   ER, with Gd, U-73122 or TG, cell migration toward the plate center was significantly

245   reduced compared with control group, which was the same as the removal of

246   extracellular calcium ions with Ca^{2+}-free medium (Fig. 4F; Supplementary Movies S4

247   to S7). For MSCC- and ER-blocking groups, cell migration along flow direction was

248   enhanced (Fig. 4G), indicating that RAW264.7 cells lose the sensitivity for the

249   gradient FSS.

250

251   **Other Four Types of Cells Don't Migrate along the Gradient of FSS**

252   To examine whether gradient FSS-dependent cell migration is unique for

253   osteoclast precursors or not, further experiments were performed for other four types

254   of cells, i.e. MC3T3-E1, PDLF, rMSC and MDCK (Fig. 5A; Supplementary Movies

255   S8 to S11). Under static condition, these cells did not reveal any tendency of

256   migrating along radial or circumferential directions (Figs. 5B and 5C). After being

257   exposed to fluid flow, only rMSC migrated toward the center within 40 min with

258   significantly longer distance than MC3T3-E1, PDLF and MDCK, however, obviously

259   less than RAW264.7 cells. The migration of RAW264.7, PDLF and rMSC along

260   circumferential direction after flow stimulation was significantly enhanced compared

261   with static condition, and the circumferential migration distance of PDLF and rMSC

262   was significantly higher than RAW264.7 (Fig. 5C).The above results reveal that

263   PDLF and rMSC tend to migrate along flow direction rather than radial direction,

264   indicating they are not sensitive to gradient FSS.

265

RAW264.7 Cells Tend to Aggregate and Differentiate in Low-FSS Region

To study the effect of gradient FSS-dependent migration on cell aggregation and differentiation, RAW264.7 cells were cultured in the cone-and-plate flow chamber system for 6 days and were exposed to flow stimulation for 1 h three times each day. The images at different distances relative to the plate center were captured at different times (Fig. 6A), and the number of cells was counted (Fig. 6B). When cells were cultured initially without fluid flow, no significant difference was observed for the cell number at different locations, approximately 104–120 cells in the field of view. At 3 days after flow stimulation, the cell number increased to about 160 at the center or 4 mm away from the center, which was significantly higher than 109 at the outer region of 8 mm to the center. After 6 days of culture and flow stimulation, the tendency of cell aggregation at the center became more evident and the cell number at the center was 364, which was considerably higher than 232 at the outer region. This higher level of cell density at the center may be due to cell migration toward the low-FSS region.

To examine whether the fusion of RAW264.7 cells was also associated with FSS gradient or cell aggregation, the mature osteoclast marker TRAP and cell nuclei were stained and the images were taken at different locations and times (Figure 7A); the TRAP-positive cells with more than two nuclei were regarded as osteoclasts. Figure 7B shows the multinucleated osteoclasts at different distances of 0, 4 and 8 mm to the center before or 3 days and 6 days after flow stimulation. At the center of a well with a radius less than 4 mm, the percentage of multinucleated cells was highest up to 7.9%–8.8%, which was consistent with our previous work (9, 18). The ratio of fusion decreased with the increase of distance to the center (e.g., 3.3% at 8-mm region). Therefore, we could speculate that RAW264.7 cells were more likely to fuse into multinucleated osteoclasts in the low-FSS region.

12

291

Discussion

293   In the present study, we constructed a gradient FSS field by using a custom-made

294   cone-and-plate flow chamber system (Fig 2). Cone–plate configuration has been

295   frequently used as viscometer in biomedical research, through which the rotation of a

296   cone with linear generatrix may cause uniform FSS field (22). In the past several

297   decades, cone–plate apparatus similar to cone-and-plate viscometer have been used to

298   study uniform FSS on the adherent cells, however, only a few studies have been

299   conducted about the effect of gradient FSS on biological behavior of cells (23-26). For

300   example, Yan et al. adopted microfluidic technology to construct gradient FSS field and

301   demonstrated that tumor cells prefers to adhere and grow at low-FSS region (i.e., the

302   inner side of curved microvessels) (26). To the best of our knowledge, the gradient

303   FSS field for the cone-and-plate system and its effect on cell migration have yet to be

304   investigated.

305   In the early 1960s, Cox discovered that the direction of fluid flow in a cone–plate

306   apparatus deviates circumferential direction, which is called as secondary flow (22).

307   Some following theoretical analyses showed that at sufficiently low shear rate, the

308   secondary flow is negligible and the primary flow along the circumferential direction

309   provides a good approximation to the flow (23, 27). In addition, Sdougos et al. defined

310   a non-dimensional Reynolds number $\mathrm{Re} = \rho \omega h^2 / (12 \nu)$, in which ρ is the density of

311   medium, ω is the angular velocity, and ν is the dynamic viscosity (28). The authors

312   found that when Re was less than 0.5, the flow case was laminar flow; however,

313   secondary flow would occur when Re was between 0.5 and 4.0. Recently, analytical

314   and numerical analyses have described the steady, laminar, three-dimensional flow of

315   a Newtonian fluid at low Reynolds numbers on endothelial cells (29). In the present

13

316   study, Re was calculated as 0.06 considering that the height of the cone at the radius

317   of 8 mm was 0.2 mm, and the flow case should be laminar flow. In fact, the

318   cone-and-plate flow chamber designed in this study modified the cone's shape; that is,

319   the cone's generatrix was not as linear as the traditional cone–plate apparatus adopted.

320   This novel cone–plate flow chamber caused secondary flow, whose angle to

321   circumferential direction was less than 8.3^{o}, which was obtained by FE numerical

322   simulation and PIV experimental test, respectively.

323   In the current work, RAW264.7 cells were exposed in a gradient FSS field ranging

324   from 0.1-0.7 Pa (Fig 3), which was the physiological level within bone cavities (21).

325   Surprisingly, cells did not migrate along the direction of fluid flow but almost move

326   toward the low-FSS region under gradient FSS stimulation for 40 min (Fig. 4). And the

327   directionality of cell migration was increased along with the time of flow stimulation

328   (Supplementary Figure S12A). To our knowledge, the phenomenon of cells sensing to

329   gradient FSS field and then migrating toward the low-FSS region have yet to be

330   reported. When we exerted the gradient FSS on other four types of cells, i.e.

331   MC3T3-E1, PDLF, rMSC and MDCK, none of them tended to migrate along radial

332   direction (Fig. 5B and 5C). PDLF and rMSC even significantly migrated along

333   circumferential direction compared with the radial component of their migration

334   distance. Therefore, it seems that RAW264.7 osteoclast precursors have a special

335   ability of sensing the direction of FSS gradient compared with other four types of cells.

336   We assume that this interesting phenomenon should be correlated with the

337   opening of mechanosensitive ion channel under fluid flow. Our previous studies

338   demonstrated that FSS induced more calcium responsive peaks in the late

339   differentiated osteoclasts than the early ones, and MSCC, PLC and ER constituted the

340   major signaling pathway (9, 18). We previously also found that when blocking the

341   pathways of MSCC, ER, or extracellular calcium, the migration of RAW264.7 cells

342   along flow direction is also significantly reduced (17). The present study showed that

343   Gd and TG significantly inhibit the migration of RAW264.7 along radial direction

344   and enhance the circumferential migration (Figs. 4F and 4G). And the directionality of

345   cell migration was significantly reduced for MSCC-, ER- or PLC- blocking groups

346   (Supplementary Figure S 12B). The above results indicate that calcium signaling

347   pathways regulate the gradient-FSS induced-migration of RAW264.7 cells. But the

348   molecular mechanism of this unique ability for RAW264.7 cells to sense gradient FSS

349   is still unknown.

350   The process of osteoclast precursors migrating to the site of bone resorption and

351   then fusing into mature multinucleated osteoclasts remains unclear. The apoptotic

352   osteocytes near a microdamage releases cytokines, such as RANKL,

353   phosphatidylserine, ICAM-3, or CD31, to regulate the recruitment and differentiation

354   of osteoclast (30-33). Aside from the above chemical factors, some researchers have

355   considered that mechanical strain in the bone matrix may regulate bone resorption.

356   For example, an *in vivo* observation has shown that the local loading direction

357   determines the tunneling orientation of osteoclasts (34). Through theoretical modeling

358   and FE analysis, the strain around a BMU resorption cavity has been studied; the

359   BMU has been predicted to move in the primary loading direction, and the osteoclast

360   activity coincides with a low-strain region (35, 36). Our present study demonstrated

361   for the first time that osteoclast precursors could sense the gradient of FSS and further

362   migrate toward low-FSS region. In addition, the ability to sense FSS gradient is

15

363   regulated by calcium channel. Finally, more monocytes fused into multinucleated

364   osteoclasts at this region. This discovery may provide a new mechanism of osteoclast

365   recruitment and differentiation during bone resorption and bone remodeling.

366   In the present study, the migration speed of cells was approximately 0.2 μm/min,

367   which may lead to the average migration distance of 0.22 mm for 6-day culture under

368   1-h flow stimulation three times each day. The area of the outer section was larger

369   than that of the inner section; thus, this inward cell migration caused more cells to

370   aggregate toward the inner region. Notably, a higher FSS level in the outer region

371   might cause more cells to be dead or detached from the substrate. However, we used

372   physiological FSS and gentle stimulation strategy (i.e.,<1 Pa and 1-h stimulation three

373   times each day); thus, abnormal adherent cells or cells suspended in the chamber were

374   not observed during the 6-day culture (Supplementary Figure S13). However, when

375   flow stimulation was applied all the time during 6 days, cell density significantly

376   decreased after 1-dayculture, and considerably few cells were observed on the plate at

377   4 days (Supplementary Figure S14).

378   In conclusion, a custom-made cone-and-plate flow chamber was adopted in this

379   study to construct a fluid flow field with gradient FSS. The experimental observation

380   revealed that RAW264.7 cells did not migrate along the flow direction but directly

381   moved toward the low-FSS region, which is regulated by calcium signaling pathways

382   of MSCC and ER. This targeted migration led to the aggregation of osteoclast

383   precursors at low-FSS region and finally enhanced their differentiation.

384

Author contributions

Y. G. and B. H. designed the research; Y. G., B. H. and J. C. performed the research; Y. G., T. Y. L., C. Y. Y. and Z. B. C. performed numerical calculations; Y. G. performed the experiment; Y. G., T. Y. L., Q. S. and M. M. G. analyzed experimental data; Y. G. and B. H. wrote the article. All authors reviewed the manuscript.

Acknowledgments

References

1. Robling, A.G., Castillo, A. B., Turner, C. H. 2006. *Biomechanical and molecular regulation of bone remodeling.* Annual Review of Biomedical Engineering. 8 (1): 455-498.

2. Wolff, S.N., Phillips, G. L., Fay, J. W. Lazarus, H. M., Herzig, R. H., Herzig, G. P. 1986. The law of bone remodelling. Berlin ; New York. XII, 126P.

3. Baroukh, B., Cherruau, M., Dobigny, C., Guez, D., Saffar, J. L. 2000. *Osteoclasts differentiate from resident precursors in an in vivo model of synchronized resorption: a temporal and spatial study in rats.* Bone. 27 (5): 627-634.

4. Norman, T.L., Wang, Z. 1997. *Microdamage of human cortical bone: Incidence and morphology in long bones.* Bone. 20 (4): 375-379.

5. Burr, D.B., Martin, R. B. 1993. *Calculating the probability that microcracks initiate resorption spaces.* Journal of Biomechanics. 26 (4-5): 613-616.

6. Eriksen, E.F. 2010.*Cellular mechanisms of bone remodeling.* Reviews in Endocrine & Metabolic Disorders. 11(4): 219-227.

7. Fazzalari, N.L., Forwood, M. R., Smith, K., Manthey, B. A., Herreen, P. 1998. *Assessment of cancellous bone quality in severe osteoarthrosis: Bone mineral density, mechanics, and microdamage.* Bone. 22 (4): 381-388.

8. Koszyca, B., Fazzalari, N. L. and B. 1989. Vernonroberts, *Trabecular microfractures - nature and distribution in the proximal femur.* Clinical Orthopaedics and Related Research. 12 (244): 208-216.

9. Li, P., Hu, M., Sun, S. J., Zhang, Y., Gao, Y. X., Long, M. A., Huo, B., Zhang, D. 2012. *Fluid flow-induced calcium response in early or late differentiated osteoclasts.* Annals of Biomedical Engineering. 40 (9): 1874-1883.

10. Bentolila, V., Boyce, T. M., Fyhrie, D. P., Drumb, R., Skerry, T. M., Schaffler, M. B. 1998. *Intracortical remodeling in adult rat long bones after fatigue loading.* Bone. 23 (3): 275-281.

11. Herman, B.C., Cardoso, L., Majeska, R. J., Jepsen, K. J., Schaffler, M. B. 2010. *Activation of bone remodeling after fatigue: Differential response to linear microcracks and diffuse damage.* Bone. 47 (4): 766-772.

12. Wang, L., Ye, T. J., Deng, L. F., Shao, J., Qi, J., Zhou, Q., Wei, L., Qiu, S. J. 2014. *Repair of microdamage in osteonal cortical bone adjacent to bone screw.* Plos One. 9 (2): e89343- e89355.

13. Waldorf, E.I., Christenson, K. B., Cooney, L. A., Goldstein, S. A. 2010. *Microdamage repair and remodeling requires mechanical loading.* Journal of Bone and Mineral Research. 25 (4): 734-745.

14. McGarry, J.G., Klein-Nulend, J., Mullender, M. G., Prendergast, P. J. 2004. *A comparison of strain and fluid shear stress in stimulating bone cell responses - a computational and experimental study.* Faseb Journal. 18 (15): 482-491.

15. Weinbaum, S., Cowin, S. C., Zeng, Y. 1994. *A model for the excitation of osteocytes by mechanical losding-induced bone fluid shear stresses.* Journal of Biomechanics. 27 (3): 339-360.

16. Thompson, W.R., Rubin, C. T., Rubin, J. 2012. *Mechanical regulation of signaling pathways in bone.* Gene. 503 (2): 179-193.

17. Liu, C.L., Li, S. N., Ji, B. H., Huo, B. 2015. *Flow-induced migration of osteoclasts and*

18

437   *regulations of calcium signaling pathways.* Cellular and Molecular Bioengineering. 8

438   (1):213-223.

439   18.   Li, P., Liu, C. L., Hu, M., Long, M., Zhang, D., Huo, B. 2014. *Fluid flow-induced calcium*

440   *response in osteoclasts: signaling pathways.* Annals of Biomedical Engineering. 42 (6):

441   1250-1260.

442   19.   Boutroy, S., Bouxsein, M. L., Munoz, F., Delmas, P. D. 2005. *In vivo assessment of trabecular*

443   *bone microarchitecture by high-resolution peripheral quantitative computed tomography.* Journal

444   of Clinical Endocrinology & Metabolism. 90 (12): 6508-6515.

445   20.   Verbruggen, S.W., Vaughan, T. J., McNamara, L. M. 2014. *Fluid flow in the osteocyte mechanical*

446   *environment: a fluid-structure interaction approach.* Biomechanics and Modeling in

447   Mechanobiology. 13 (1): 85-97.

448   21.   McAllister T. N., D., T. and F. JA, 2000. *Fluid shear stress stimulates prostaglandin and nitric*

449   *oxide release in bone marrow-derived preosteoclast-like cells.* Biochemical and Biophysical

450   Research Communications. 270 (2): 643-648.

451   22.   Cox, D.B. 1962. *Radial flow in cone-plate viscometer.* Nature. 193 (4816): p. 670-680.

452   23.   Dewey, C.F., Bussolari, S. R., Gimbrone, M. A., Davies, P. F. 1981. *The dynamic-response of*

453   *vascular endothelial-cells to fluid shear-stress.* Journal of Biomechanical

454   Engineering-Transactions of the Asme. 103 (3):177-185.

455   24.   Deyer, L.K., B. Autschbach, R. Vogt, P. Welte, T. Ngezahayo, A. Glasmacher, B. Deyer, L.

456   Krolitzki, B. Autschbach, R. 2012. *An advanced cone-and-plate reactor for the in*

457   *vitro-application of shear stress on adherent cells.* Journal of Tissue Engineering and

458   Regenerative Medicine. 6 (10): 393-393.

459   25.   Chung, C.A., Tzou, M. R., Ho, R. W. 2005. *Oscillatory flow in a cone-and-plate bioreactor.*

460   Journal of Biomechanical Engineering-Transactions of the Asme. 127 (4): 601-610.

461   26.   Yan, W.W., Cai, B., Liu, Y., Fu, B. M. 2012. *Effects of wall shear stress and its gradient on tumor*

462   *cell adhesion in curved microvessels.* Biomechanics and Modeling in Mechanobiology. 11 (5):

463   641-653.

464   27.   Fewell M. E., H.J.D. 1977. *The secondary flow of newtonian fluids in cone-and-plate viscometers.*

465   21 (2): 535-565.

466   28.   Sdougos H. P., B.S.R. and D. CF. 1984. *Secondary flow and turbulence in a cone-and-plate*

467   *device.* Journal of Fluid Mechanics, 138 (JAN): 379-404.

468   29.   Buschmann M. G., D.P. 2005. Adams N. A., Schnittler H. J., *Analysis of flow in a cone-and-plate*

469   *apparatus with respect to spatial and temporal effects on endothelial cells.* Biotechnology and

470   Bioengineering. 89 (5): 493-502.

471   30.   Al-Dujaili S. A., L., E., Al-Dujaili H., Tsang, K., Guenther A., You L. 2011. *Apoptotic osteocytes*

472   *regulate osteoclast precursor recruitment and differentiation in vitro.* Journal of Cellular

473   Biochemistry. 112 (9): 2412-2423.

474   31.   Kennedy O. D., H.B.C., Laudier D. M., Majeska R. J., Sun H. B., Schaffler M. B. 2012.

475   *Activation of resorption in fatigue-loaded bone involves both apoptosis and active*

476   *pro-osteoclastogenic signaling by distinct osteocyte populations.* Bone. 50 (5): 1115-1122.

477   32.   Cardoso L, H.B.C., Verborgt O., Laudier D., Majeska R. J., Schaffler M. B. 2009. *Osteocyte*

478   *apoptosis controls activation of intracortical resorption in response to bone fatigue.* Journal of

479   Bone and Mineral Research. 24 (4): 597-605.

480 33. Gerbaix M, G.V., Farlay D, Olivier C, Ammann P, Courbon G, Laroche N, Gential R, Follet H,
481   Peyrin F, Shenkman B, Gauquelin-Koch G, Vico L. 2017. *One-month spaceflight compromises*
482   *the bone microstructure, tissue-level mechanical properties, osteocyte survival and lacunae*
483   *volume in mature mice skeletons.* 7 (1): 2659-2671.

484 34. Petrtyl M., H.J., Fiala P. 1996. *Spatial organization of the haversian bone in man.* Journal of
485   Biomechanics. 29 (2): 161-172.

486 35. Smit T. H., B.E.H. 2000. *Is BMU-coupling a strain-regulated phenomenon A finite element*
487   *analysis.* Journal of Bone and Mineral Research. 15 (2): 301-307.

488 36. Van O. R., R.R., Tanck E. 2008. Hilbers P. A. J., Huiskes R., *A unified theory for osteonal and*
489   *hemi-osteonal remodeling.* Bone. 42 (2): 250-259.

490

491

Figure Legends
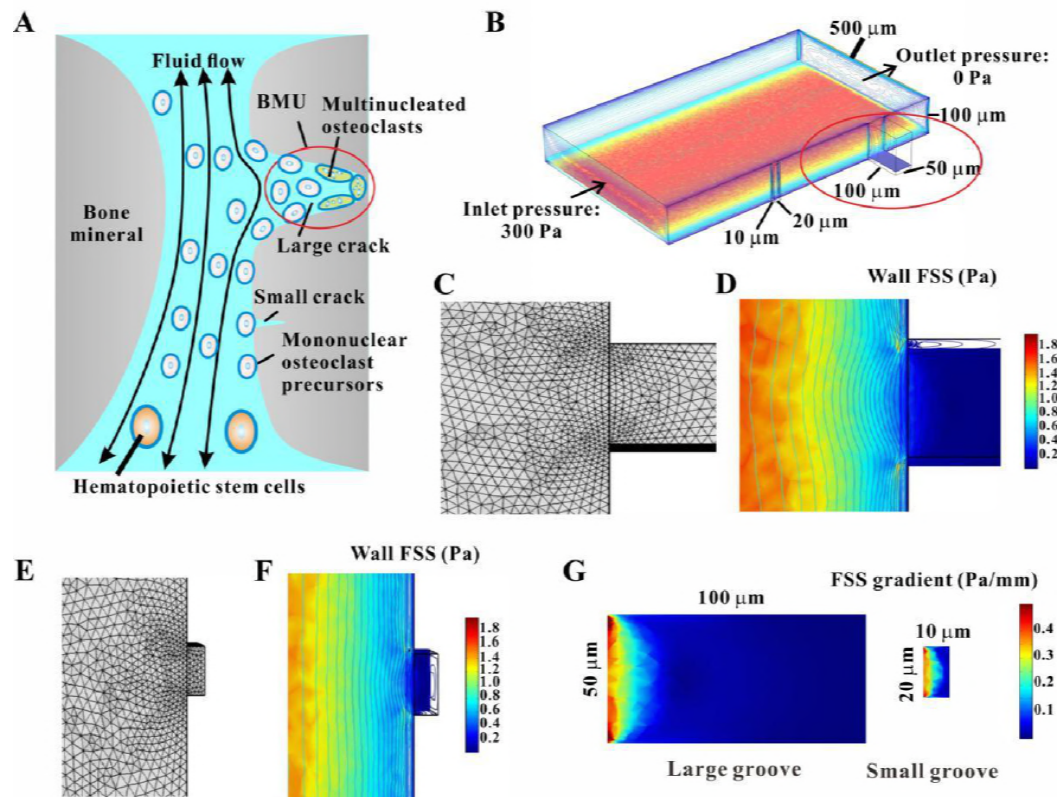
Figure 1. Fluid flow around microdamages in the cavities of trabecular bone. (A) Schematic of migration, aggregation, and fusion of osteoclast precursors around a large crack (red circle) regulated by FSS. (B) FE results of wall FSS for a fluid channel in which the grooves on the sidewall are constructed to mimic the microdamages with different sizes. The red circle indicates the region with low FSS around a large groove. FE mesh and wall FSS around the large groove are shown in (C) and (D), and those around the small groove in (E) and (F), respectively. (G) Wall FSS gradient on the bottom surface of the large and small grooves.
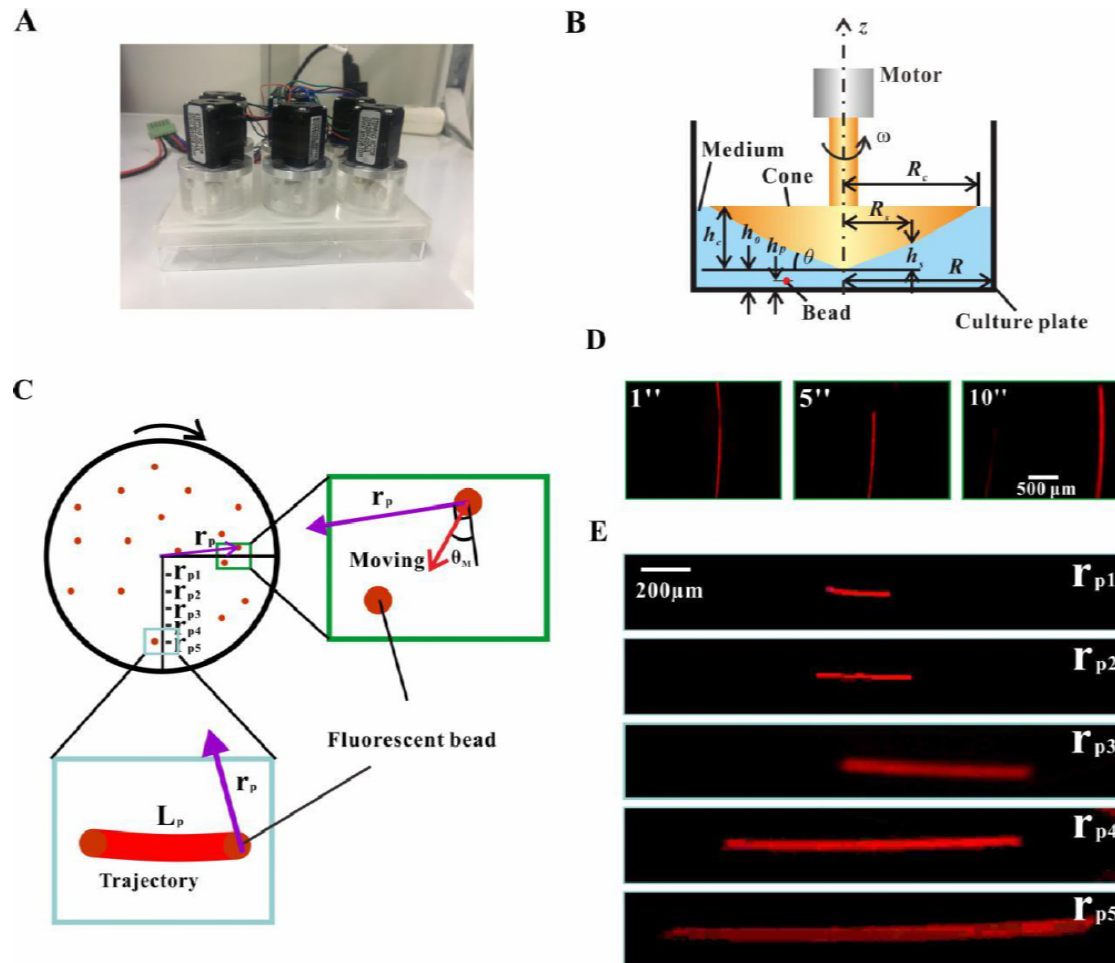
Figure 2. Cone-and-plate flow chamber and Particle Image Velocimetry. (A) Photo of the custom-made cone-and-plate flow chamber. (B) Diagram of cone-and-plate flow chamber, where h_0 is the distance of the cone's tip above the bottom of the plate, h is the height of the cone, h_p is the height of beads in a specific focal plane. θ is the angle between the cone's generatrix and the plate, ω is the angular velocity of the cone (18 rad/s), and R is the radius of the well. (C) Schematic of the analysis of PIV method, where the green and light blue boxes indicate the field of view in D and E, respectively. the orange dots are fluorescent beads, rp is the distance between fluorescent beads to the well's center (r_{p1}, r_{p2}, r_{p3}, r_{p4} and r_{p5} denote the locations of 2 mm, 4 mm, 6 mm, 8 mm and 10 mm away from the center, respectively), and θ_M is the angle between the actual flow directions (red arrow) indicated by beads' movement and the circumferential directions. Red line means the beads' trajectory. (D) Traces of fluorescent latex beads recorded at different times (6 mm from the center, time of exposure is 50 ms, h_p is 0.2 mm). (E)Traces of fluorescent beads recorded at different location (time of exposure is 20 ms, h_p is 0.1 mm).
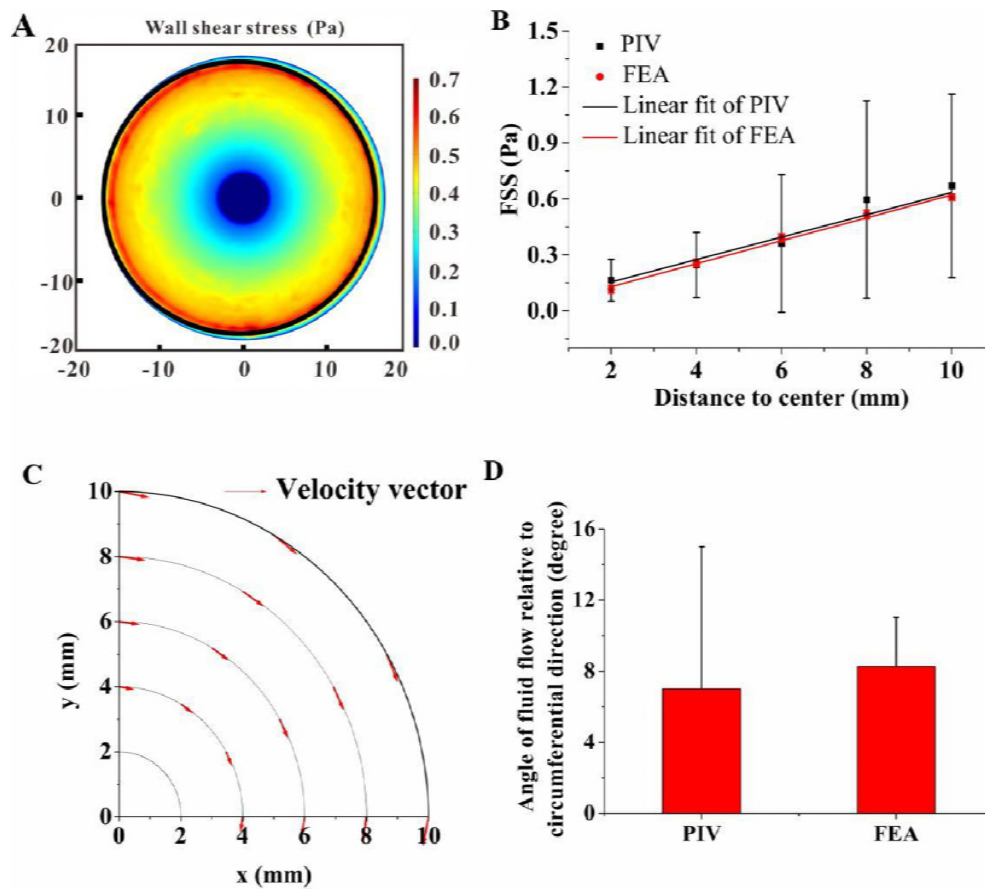
Figure 3. Finite element analysis (FEA) of fluid flow and comparation with PIV measurements. (A) Numerical simulation results of wall FSS on the surface of one well. (B) Wall FSS at different distance away from the center, in which the linear regression parameters for numerical simulation and PIV measurement are R=0.9979 and R=0.94553, respectively. (C) Velocity vectors (red arrows) indicating secondary flow against circumferential direction. (D) Angle of the direction of fluid flow relative to circumferential direction measured by PIV and predicted by FEA.
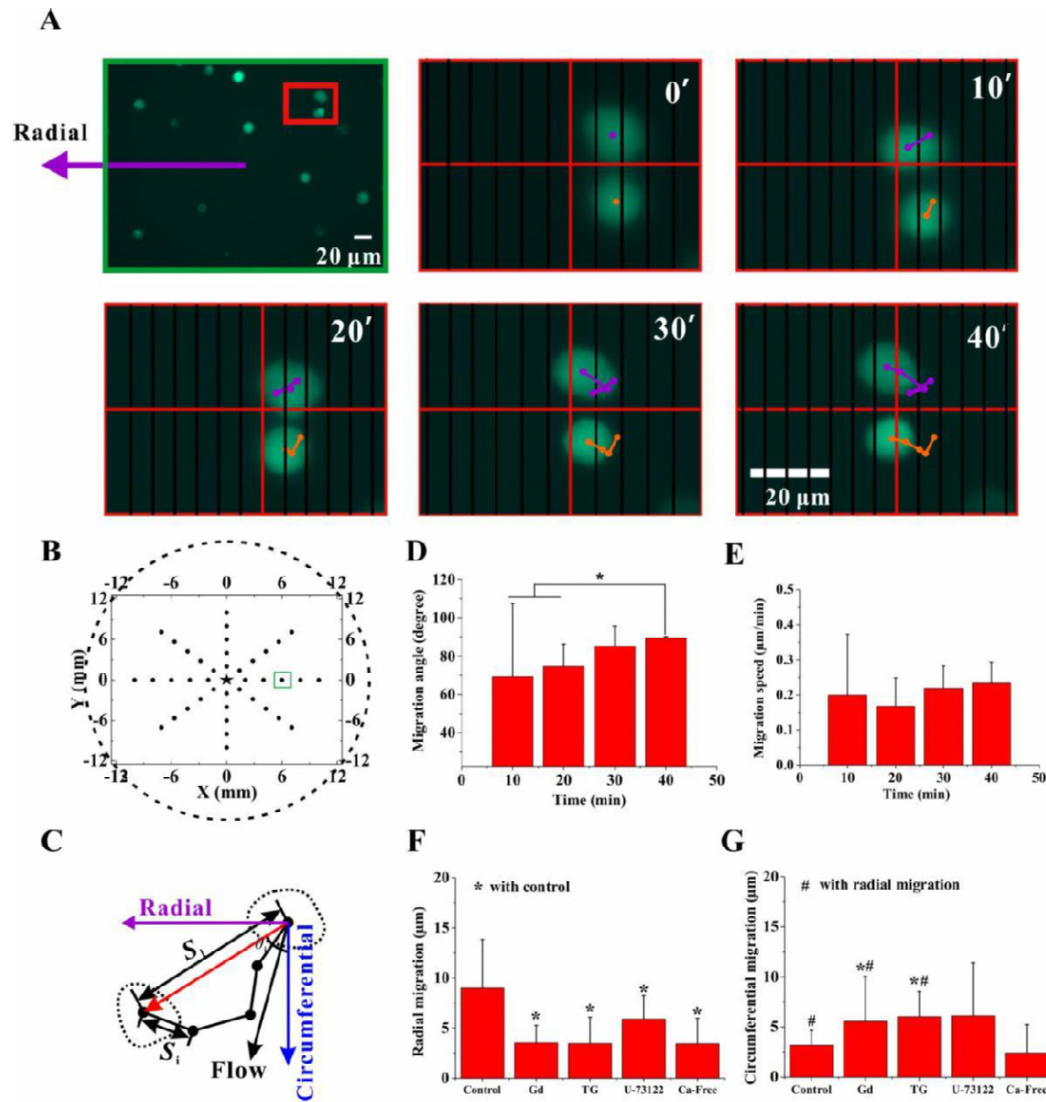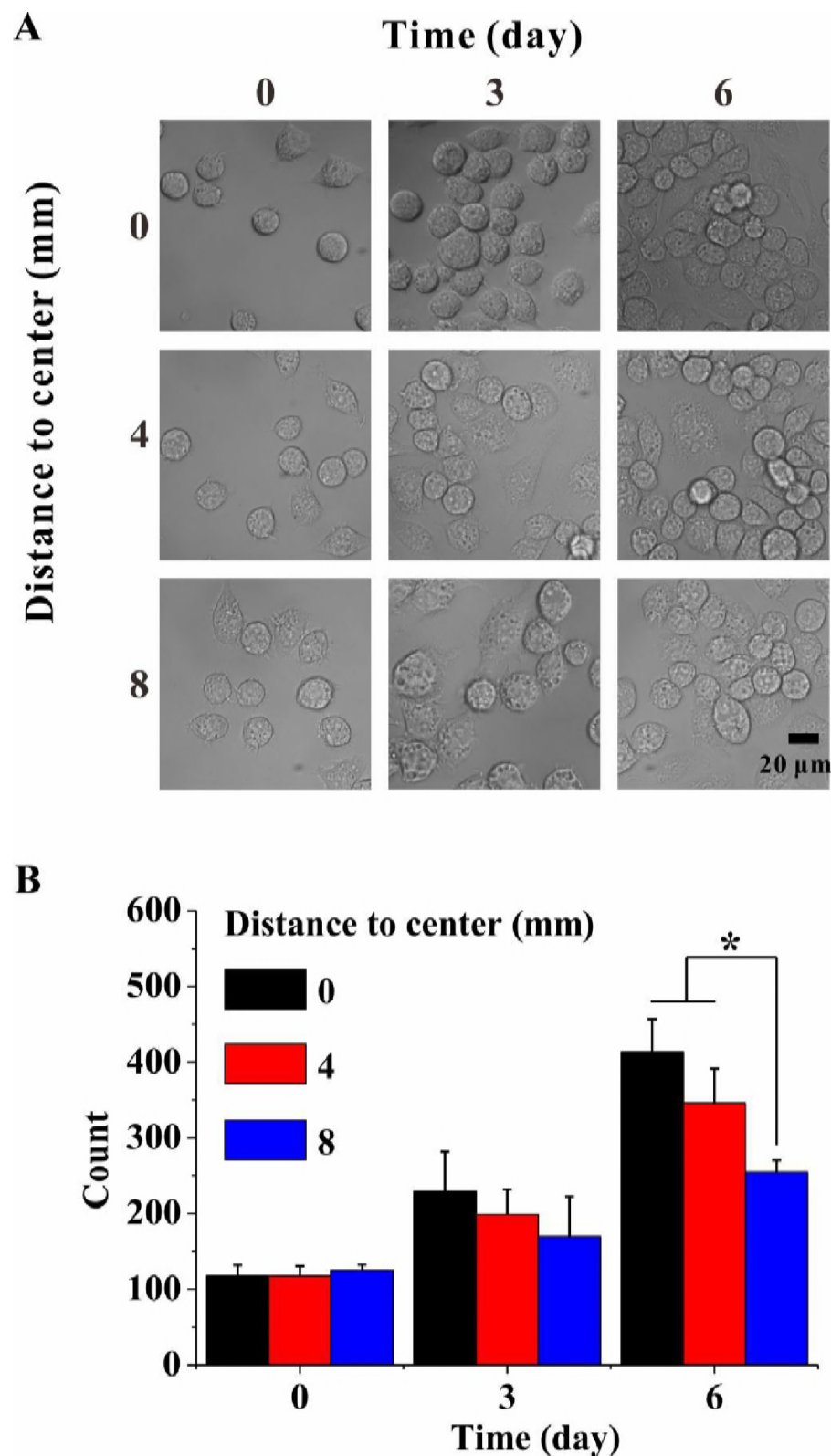
Figure 4. Cell migration under gradient FSS. (A) RAW264.7 cells stained with Oregon Green. The migration of the cells within a red box in the first image is shown in five time-lapsed images. The red and black lines are for the positioning of cell migration. (B) Positioning marks (black dots) in a well (dotted circle) of a six-well culture plate used for the multistage module of inverted fluorescence microscope. The black star marks the plate center. The green box indicates the field of view in A. (C) Definition of migration parameters. The black dots indicate the centroids of a migrating cell at different time. S_i is the distance of cell movement in a given time interval, S_l is the distance of a cell away from its initial position in a given time, and θ_i is the angle between circumferential direction and migration directions of one cell relative to its initial position. (D) Migration angle θ_i of cells in a given time interval. (E) Migration speed of cells in a given time interval. The effect of calcium signaling pathways on migration distance along radial (F) and circumferential (G) directions, respectively. *, #, p<0.05.
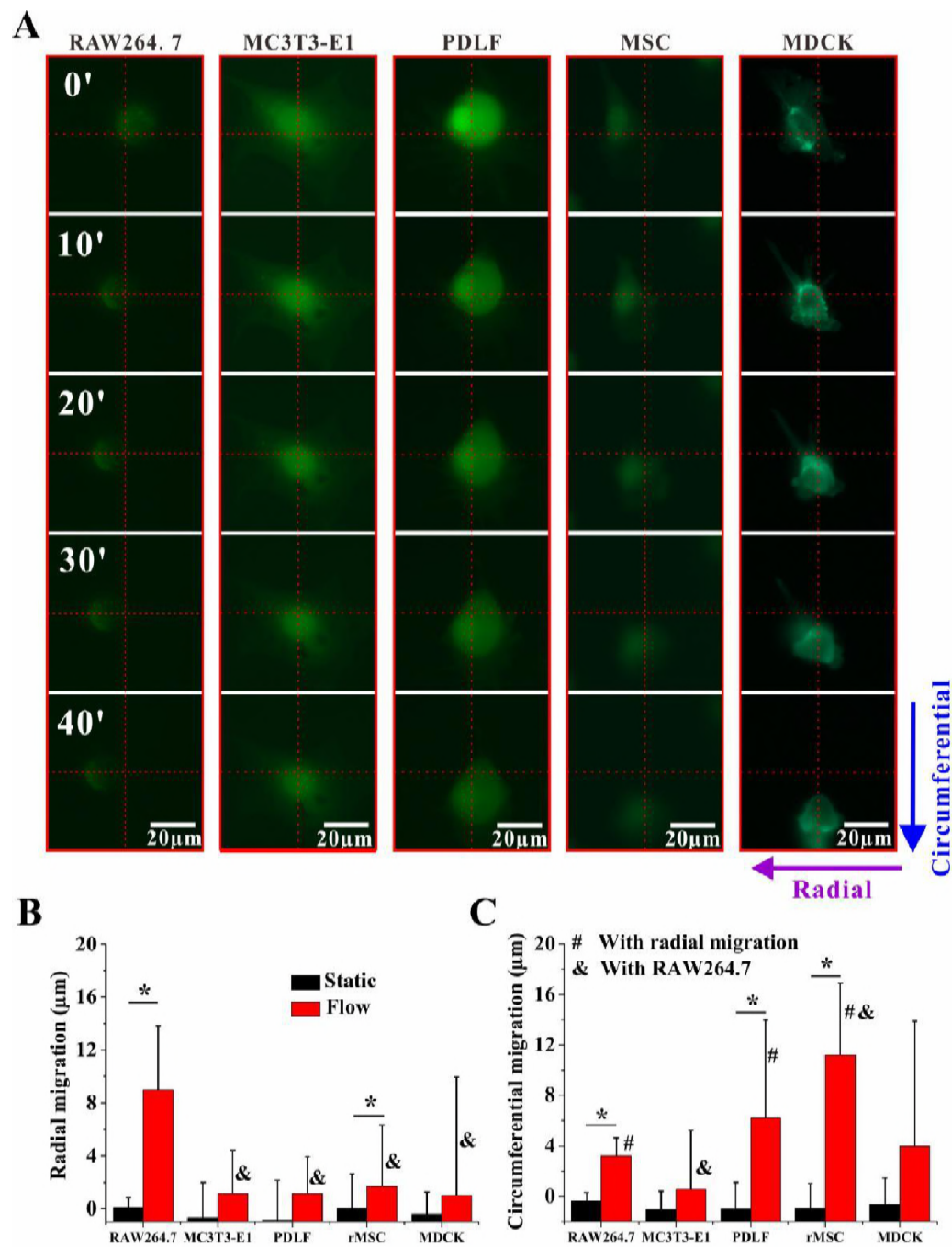
Figure 5. Migration of RAW264.7, MC3T3-E1, PDLF, rMSC and MDCK cells under gradient FSS. (A) The time-lapsed fluorescent images of migrating cells stained with Oregon Green. (B, C) The distance of cells migration along radial and circumferential directions, respectively. *, &, #, $p<0.05$.

Figure 6. Cell aggregation under gradient FSS. (A) Photos of RAW264.7 cells at different distances to the center when being cultured for different times under 1-h fluid flow stimulation performed three times each day. (B) Average number of cells in the field of view. *, p<0.05.
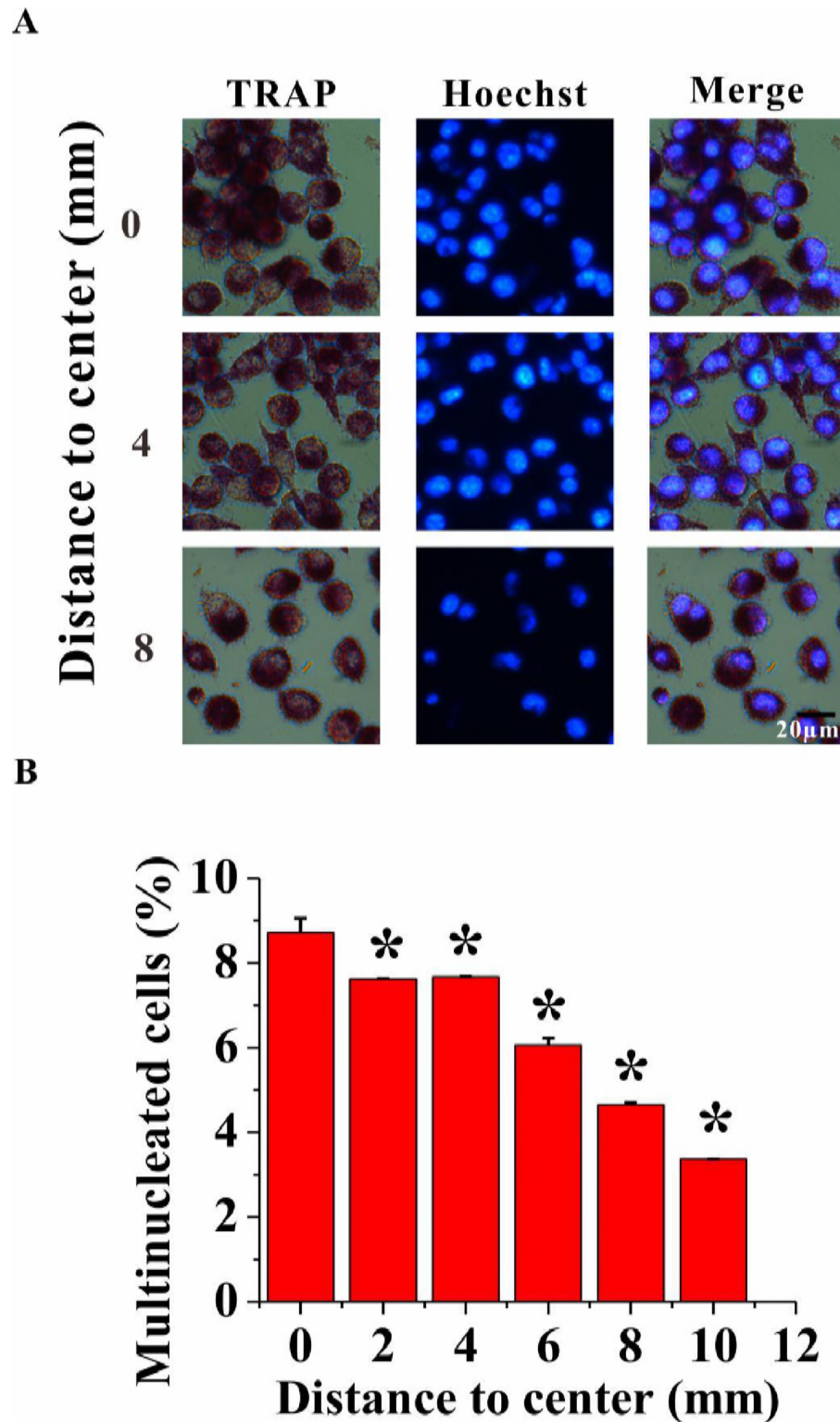
Figure 7. Cell differentiation under gradient FSS. RAW264.7 Cells were induced for differentiation by RANKL and M-CSF, and mechanically stimulated with gradient FSS up to 6 days, during which 1-h fluid flow stimulation was performed three times each day. (A) Images of RAW264.7 cells with nuclear staining by Hoechst and TRAP staining. (B) Percentage of multinucleated cells at different distances to the center. *, p<0.05.